Taylor & Francis
Taylor & Francis Group

🔓 OPEN ACCESS | Check for updates

Enhancing T-cell recruitment in renal cell carcinoma with cytokine-armed adenoviruses

Michaela Feodoroff[a,b,c,d,e], Firas Hamdan[a,c,d], Gabriella Antignani[a,c,d], Sara Feola[a,c,d], Manlio Fusciello[a,c,d], Salvatore Russo[a,c,d], Jacopo Chiaro[a,c,d], Katja Välimäki[b], Teijo Pellinen[b,e], Rui M. Branca[f], Janne Lehtiö[f], Federica D´alessio[a,c,d], Paolo Bottega[a,c,d], Virpi Stigzelius[a,c,d], Janita Sandberg[a,c,d], Jonna Clancy[g], Jukka Partanen[g], Minna Malmstedt[e,h,i], Antti Rannikko[e,h,i], Vilja Pietiäinen[b,e], Mikaela Grönholm[a,c,d,e], and Vincenzo Cerullo [iD][a,c,d,e,j]

aLaboratory of Immunovirotherapy, Drug Research Program, University of Helsinki Faculty of Pharmacy, Helsinki, Finland; bInstitute for Molecular Medicine Finland (FIMM), Helsinki Institute for Life Sciences (HiLIFE), University of Helsinki, Helsinki, Finland; cTRIMM,Translational Immunology Research Program, University of Helsinki, Helsinki, Finland; dDrug Delivery, Drug Research Program, Division of Pharmaceutical Biosciences, Faculty of Pharmacy, University of Helsinki, Helsinki, Finland; eiCAN Digital Precision Cancer Medicine Flagship, University of Helsinki, Helsinki, Finland; fScience for Life Laboratory, Department of Oncology-Pathology, Karolinska Institutet, Solna, Sweden; gDepartment of Research and Development, Finnish Red Cross Blood Service, Helsinki, Finland; hDepartment of Urology, Helsinki University Central Hospital, Helsinki, Finland; iHUS, University of Helsinki, Helsinki, Finland; jDepartment of Molecular Medicine and Medical Biotechnology and CEINGE, Naples University 24 Federico II, Naples, Italy

ABSTRACT

Immunotherapy has emerged as a promising approach for cancer treatment, with oncolytic adenoviruses showing power as immunotherapeutic agents. In this study, we investigated the immunotherapeutic potential of an adenovirus construct expressing CXCL9, CXCL10, or IL-15 in clear cell renal cell carcinoma (ccRCC) tumor models. Our results demonstrated robust cytokine secretion upon viral treatment, suggesting effective transgene expression. Subsequent analysis using resistance-based transwell migration and microfluidic chip assays demonstrated increased T-cell migration in response to chemokine secretion by infected cells in both 2D and 3D cell models. Flow cytometry analysis revealed CXCR3 receptor expression across T-cell subsets, with the highest percentage found on CD8+ T-cells, underscoring their key role in immune cell migration. Alongside T-cells, we also detected NK-cells in the tumors of immunocompromised mice treated with cytokine-encoding adenoviruses. Furthermore, we identified potential immunogenic antigens that may enhance the efficacy and specificity of our armed oncolytic adenoviruses in ccRCC. Overall, our findings using ccRCC cell line, *in vivo* humanized mice, physiologically relevant PDCs in 2D and patient-derived organoids (PDOs) in 3D suggest that chemokine-armed adenoviruses hold promise for enhancing T-cell migration and improving immunotherapy outcomes in ccRCC. Our study contributes to the development of more effective ccRCC treatment strategies by elucidating immune cell infiltration and activation mechanisms within the tumor microenvironment (TME) and highlights the usefulness of PDOs for predicting clinical relevance and validating novel immunotherapeutic approaches. Overall, our research offers insights into the rational design and optimization of viral-based immunotherapies for ccRCC.

Introduction

The complex human immune system is highly organized and vital for constantly monitoring health threats, pathogens and preventing cancer development. Conventional cancer treatments like surgery effectively manage local tumor control but tend to inadequately target metastases. While immunotherapy has already been successful in treatment of many tumor types, including metastatic ccRCC, there is a pressing need for improved recognition of the patients who benefit of these therapies to achieve durable tumor control.

Immune checkpoint inhibitor therapy (ICIT) has long been recognized for enhancing cancer cell recognition and attack by circulating immune cells[1]. T-cell infiltration linked with progression-free survival underscores the significance of effector-to-target cell ratios in tumor immunity.[2] Adequate intratumoral distribution and presence of CD8+ and CD4+ T-cells has furthermore been shown to correlate with favorable clinical outcomes and success of cancer immunotherapy.[2,3]

Chemokines, a subfamily of cytokines, play a crucial role in regulating immune cell infiltration, movement within the TME and interplay with other (immune) cells.[4] Inadequate chemokine signaling and distribution in the TME contribute to tumor progression by limiting the presence of immune effector cell populations responsible for antitumor immunity. Especially CXCL9 (MIG) and CXCL10 (IP-10) chemokines are associated with this process. The corresponding chemokine receptor, CXCR3, expressed on activated CD4+ and CD8+ T-cells, Th1 cells, and NK cells is associated with effector mechanisms of the adaptive immune response[5,6] and correlated with T-cell infiltration in solid tumors,

including RCC, melanoma, and ovarian cancer.[4] Interleukin 15 (IL-15), a cytokine involved in regulating the immune system´s response to inflammation and infection, is known to stimulate activation and proliferation of T- and NK cells and promote survival of CD8+ memory T-cells.[7,8] Therefore, it renders as a promising candidate for cancer vaccines.

Oncolytic adenoviruses, serving as widely used viral vectors for cancer immunotherapy, are genetically modified to act as gene transfer vehicles, enabling selective targeting of malignant cells. They induce anticancer mechanisms through multiple pathways including virus-mediated tumor cell lysis,[9,10] thereby mediating a release of tumor-associated antigens recognized by antigen-presenting cells, consequently promoting tumor-specific T-cell responses.

In this study, we demonstrate the effect of oncolytic adenoviruses armed with CXCL9, CXCL10 and IL-15 to 1) infect cancer cells, 2) secrete the encoded proteins and 3) drive gradient-dependent T-cell attraction in vitro. Our in vivo validation further showed a greater intratumoral infiltration of CD3+, CD4+ and CD8+ T-cells, as well as NK-cells, following treatment with armed viruses compared to control groups. Finally, ccRCC cells were screened for tumor-specific peptides, identifying two superior candidates for further validation of their immunogenicity in a (personalized) oncolytic cancer vaccine approach, previously referred to as PeptiCRAd.[11]

Materials and methods

Cell lines

The human clear cell renal adenocarcinoma cell-line 786-O (American Type Culture Collection (ATCC)) was cultured in RPMI (Roswell Park Memorial Institute, Gibco, Cat#21875034) medium supplemented with 10% fetal bovine serum (FBS) (Thermo Fisher Scientific, Cat#10500064), 1% GlutaMAX (Thermo Fisher Scientific, Cat#35050038), and 1% penicillin–streptomycin (10,000 U/mL) (Gibco, Cat#15140122) at +37°C and 5% CO_2.

Patient-derived cell cultures

PDCs derived from three different clinically diagnosed ccRCC patients (Pt-1, Pt-2 and Pt-3) were cultured in 3:1 (v/v) Ham´s F-12 Nutrient mix (Gibco, Cat#11765054) and DMEM (Gibco, Cat#11965092) supplemented with 5% FBS, 8,4 ng/mL Choleratoxin (Sigma, Cat#C8052), 0.4 µg/mL hydrocortisone (Sigma, Cat#H4001), 10 ng/mL epidermal growth factor (Corning, Cat#354052), 24 µg/mL Adenine (Sigma, Cat#A8626), 5 µg/mL insulin (Sigma, 91077C) and 10 µM of Y-27632 RHO inhibitor (Sigma, Cat#SCM075). Patient-derived 2D and 3D cell cultures were maintained on 2% and in 20% Matrigel, respectively.

Oncolytic adenoviruses

Oncolytic adenovirus5-Δ24 (Ad5-Δ24) expressing red fluorescence protein (Ad5-Δ24-RFP) was used to visually model the viral infectivity in PDOs. In addition, we used adenovirus5/3-Δ24 (Ad5/3-Δ24) with its armed versions expressing human cytokines CXCL9 (Ad5/3-CXCL9), CXCL10 (Ad5/3-CXCL10) and IL-15 (Ad5/3-IL-15) generated as previously described.[12]

ELISA

Cells were plated on 96-well plates at 1×10^5 cells/well and infected with Ad5/3-CXCL9, Ad5/3-CXCL10 and Ad5/3-IL-15 viruses at multiplicity of infection (MOI) of 100. The concentrations of each cytokine, CXCL9, CXCL10 and IL-15 were determined in the cell culture supernatant 72 h after infection, and in animal tumors collected at the experimental endpoint by ELISA (MIG/CXCL9 human ELISA kit (Thermo Fisher Scientific, Cat#EHCXCL9), Human IP-10 ELISA kit (Abcam, ab83700) and IL-15 human ELISA kit (Thermo Fisher Scientific, Cat#BMS2106)).

MTS cell viability assay

Cells were seeded at 1×10^4/well on 96-well plates and infected with Ad5/3-Δ24, Ad5/3-CXCL9, Ad5/3-CXCL10 and Ad5/3-IL-15 at 10-fold increasing concentrations (0 to 1000 viral particles (vp) per cell) for 72 h incubation or at MOI 10 for 48 h with- or without anti-PD-1 (BioXCell Cat#BE0188), prior to assay development according to the manufacturer´s protocol (CellTiter 96 AQueous One Solution Cell Proliferation Assay; Promega, Nacka, Sweden). Varioskan LUX Multimode Reader (Thermo Fisher Scientific, Carlsbad, CA, USA) operated by SkanIt software was used for acquirement of the spectrophotometric data.

TCID$_{50}$ assay

The TCID$_{50}$ dose was assessed by plating and infecting 1×10^4 cells on 96-well plates with serially diluted viruses (Ad5/3-Δ24, Ad5/3-CXCL9, Ad5/3-CXCL10 and Ad5/3-IL-15) for 24 h, 48 h, 72 h and 96 h incubation at +37°C and 5% CO_2. Cell viability was detected according to the manufacturer's protocol (CellTiter 96 AQueous One Solution Cell Proliferation Assay; Promega, Nacka, Sweden) with Varioskan LUX Multimode Reader. TCID$_{50}$ values were calculated using the Reed-Muench formula $I = [(\%$ of wells infected at dilution above $50\% - 50\%)/(\%$ of wells infected at dilution above 50% - % of wells infected at dilution below 50%)$]$ and the 50% endpoint titer = 10log total dilution above 50%-$(^I$ x log$(^h))$, where I is the interpolated value of the 50% endpoint and h is the dilution factor.

PBMC purification

PBMCs from healthy-donor buffy coats were isolated by double density isolation method in a 1:1 ratio of PBS diluted blood and Ficoll (Sigma Cat#GE17-1440-02). PBMCs were collected after two rounds of centrifugation, first at 400×g for 30 min and then at 400×g for 10 min at room temperature. Red blood cells were lysed using ACK Lysing Buffer (Gibco, Cat#11509876) and removed by centrifugation. Remaining PBMCs were resuspended in supplemented RPMI medium.

Transwell assay

A total of 1×10^5 PBMCs were plated in a 24-well plate on top of target cells infected at MOI 100 with Ad5/3-Δ24, Ad5/3-CXCL9, Ad5/3-CXCL10 and Ad5/3-IL-15 viruses, or their combinations. Purified CXCL10 chemokine (Thermo Fisher Scientific, Cat#RP-87841) was alternatively plated at increasing concentrations on the well bottom. 1×10^5 or 1×10^4 purified human PBMCs were fluorescently labeled with 5 µM CellTracker™ Green CMFDA Dye (Thermo Fisher Scientific, Cat#C2925) according to the manufacturer´s protocol and added onto 6.5 mm transwell® Polycarbonate Membrane Inserts with 5.0 µm or 8.0 µm pore size prior to 72 h or 3 h incubation, respectively. Migrated PBMCs were detected with BD LSRFortessa (BD Biosciences) using Precision Count Beads™ (BioLegend, Cat#424902).

Microfluidic chip assay

Microfabrication of organoid-on-chip platform in polydimethylsiloxane (PDMS, Momentive, UK) was carried out via replica molding by Finnadvance. A 10:1 (by weight) ratio of base to curing agent was used, and the resulting material was cured at 65°C for 4 h. The two parts were bonded to a glass slide using PDMS slurry and were allowed to bake for another 4 h at 65°C. The chips were rinsed with 96% ethanol and UV sterilized prior to use. Purified CXCL10 chemokine or Pt-2 PDOs were plated in PDO sample chambers and infected with Ad5/3-Δ24, Ad5/3-CXCL9, or Ad5/3-CXCL10 adenoviruses at MOI 100 or left uninfected (MOCK). 1×10^4 PBMCs stained with 5 µM CellTracker™ Green CMFDA Dye (Thermo Fisher Scientific, Cat#C2925) were added to the fluidics chamber and their migration was followed for 3 h or overnight on a rocking surface or 72 h at +37°C and 5% CO_2. Images were obtained using the Invitrogen™ EVOS M7000 Cell Imaging System (Thermo Scientific) microscope. The number of migrated PBMCs was quantified by ImageJ software.

Alternatively, a commercially available AKITA microfluidics platform (Plate96-Single 10 µm pore size) from Finnadvance was used for chip migration assays to analyze the cell line and PDCs in parallel. In this setup, 20,000 cells from the 786-O cell line or Pt 1–3 cells were plated in 20% Matrigel and allowed to develop into organoids over 1 week. The organoids were then harvested and infected with Ad5/3-Δ24, Ad5/3-CXCL9, or Ad5/3-CXCL10 adenoviruses at MOI 100, or left uninfected (MOCK). After infection, 10% Matrigel was added, and the organoids were plated on top of the filter in the AKITA plate. Next, 5×10^4 PBMCs were stained with 5 µM CellTracker™ Green CMFDA Dye and added to the flow channel. The plate was then incubated on a rocker at 1 rpm at 20° tilting angle for 72 h (AKITA, Finnadvance). Migrated cells were imaged at various time points using the Invitrogen™ EVOS M3000 Cell Imaging System (Thermo Scientific) and quantified with Celleste 6.01 software (Thermo Scientific).

Animal experiment

About 4-6-week-old female B-NDG Knockout mice (NOD. CB17-Prkdcscid IL2rgtm1/BcgenHsd) were purchased from ENVIGO (Laboratory, Bar Harbor, Maine, UK). Human ccRCC (786-O) tumors were established by subcutaneously injecting 5×10^6 cells into each flank. To increase tumor size, an additional 10×10^6 786-O cells were injected adjacent to the already engrafted tumors to increase their size before intratumoral treatment with 1×10^9 viral particles in 30 µL or 100 µg of anti-human PD-1 (Bio X Cell Cat# BE0188, RRID: AB_10950318) intraperitoneally in 100 µL. 5×10^6 healthy-donor human PBMCs were injected intraperitoneally in 100 µL. Tumor size was measured every 2–3 days and tumor volume was calculated using the following formula: ((long side)×(short side)^2/2. All mice were sacrificed 12–18 days after the second tumor implantation.

Flow cytometry

Antibodies used for sample stainings include the following:

In vitro: Alexa Fluor 700 CD3 (eBioscience Cat#56-0038-80), APC anti-human CD274 (B7-H1, PD-L1, BioLegend Cat#329708), APC anti-human CD4 (BioLgened Cat#357408), APC/Cyanine7 anti-human CD183 (CXCR3) (BioLegend Cat#353722), FITC anti-human CD4 (BioLegend Cat#300506), FITC anti-human CD8 (BioLegend Cat#344704), PE anti-human CD8b (Ly-3) (BioLegend Cat#126608), PE anti-human HLA-A,B,C (BioLegend Cat#311406), Human TruStain FcX (BioLegend Cat#422302).

In vivo: PE-Cy7 anti-human CD3 (BioLegend Cat#300316), Alexa Fluor 700, eBioscience, CD3 Monoclonal Antibody (Thermo Fisher Scientific Cat# 56-0038-80), Brilliant Violet 421 anti-human CD3 (BioLegend Cat#344834), PECy5 anti-human CD4 (BioLegend Cat#317411), FITC anti-human CD4 (BioLegend Cat#300506), APC anti-human CD8a (BioLegend Cat#301014), PE/Cyanine5 anti-human CD8 (BioLegend Cat#344770), APC/Cyanine7 anti-human CD183 (CXCR3) (BioLegend Cat#353722), PE anti-human CD56 (BioLegend Cat#318306), Human TruStain FcX (BioLegend Cat#422302).

Flow cytometry data was acquired using BD LSRFortessa (BD Bioscience) and analyzed with FlowJo software version 9.

Histological tissue processing

Fixed tissues were processed using KOS Multifunctional Microwave Tissue Processor and paraffin embedded with Microm EC 350 Modular tissue embedding center (Thermo Fisher Scientific) prior to histological staining. Tissues were sliced at 4 µm sections on Superfrost objective slides (Kindler O Gmbh).

Multiplex immunohistochemistry

Formalin-fixed paraffin-embedded (FFPE) tumor sections were prepared for multiplex immunohistochemistry (mIHC) staining by deparaffinization and rehydration in xylene and ethanol series, respectively followed by antigen retrieval and peroxide (0.9% $H2O2$) and protein (10% goat serum (Gibco Cat#16210064)) blockade. mIHC staining was performed in two cycles with the following antibodies and fluorescence labels for round 1; DAPI (white) (Roche, #10236276001), FOXP3 (green) (Abcam, ab20034), CD3

(orange) (Thermo Fisher Scientific, MA5–14482), CD4 (blue) (Abcam, ab133616), CD8 (red) (Dako, M7103), and round 2; CD45 (red) (Dako M0701) and CAIX (Novus Biologicals, NB100–417) + E cadherin (Cell Signaling Technology, cst 3195) + pan Cytokeratin (Abcam, ab9377) (blue) and scanned with Zeiss Axio Scan Z.1 with 20× (NA 0.8). Zen Microscopy software (ZEISS) was used for obtaining all images.

Immunofluorescence staining

PDCs were dissociated using Gentle cell dissociation media and plated in 2D on 2% Matrigel coated wells while PDOs were plated in 20% Matrigel on 8 well Nunc; Lab-Tek; II Chamber Slides and allowed to grow for 4 days. Cells were fixed with 4% paraformaldehyde, permeabilized using 0.1% or 0,05% Triton-X100, respectively, and stained for CAIX (Novus Cat#NBP1 -51,691, RRID:AB_11011250), Vimentin (2D1) (Novus, Cat#92 687AF647), pan Cytokeratin (AE-1/AE-3) (Novus Cat#NBP2-33200AF750, RRID:AB_2868569), E-Cadherin (Novus, Cat#NBP2 -67,540), Alexa Fluor 633 Phalloidin (Invitrogen, Cat#A22284) and DAPI (Sigma). Microscopy pictures were taken using the Invitrogen™ EVOS M7000 Cell Imaging System (Thermo Scientific) and 2D deconvolution was performed with Celleste 6.01 software (Thermo Scientific).

HLA-typing

786-O cell line has previously been HLA-typed by Scholtalbers et al.[13] HLA-typing of PBMCs from healthy donors was performed by the Finnish Red Cross Blood Service using sequencing-based clinical-grade typing methods.

Peptide purification

Snap-frozen cell pellets containing 1×10^8 cells underwent a 2 h incubation at 4°C in lysis buffer (150 mm NaCl, 50 mm Tris-HCl (pH 7.4), supplemented with protease inhibitors (A32955, Thermo Scientific Pierce, Waltham, MA), and 1% Igepal (I8896, Sigma-Aldrich, St. Louis, MO). Sample lysis was followed by 1) low-speed centrifugation for 10 min at 500×g and 2) 30 min centrifugation at 25,000×g. Cleared lysate was loaded into an immunoaffinity column (AminoLink Plus Immobilization, Thermo Fischer Scientific) where 2 ml of pre-packed Agarose Resin was covalently linked to 1 mg of W6/32 antibody (inVivoMAb, BioXCell) using a linking procedure at neutral pH (pH = 7.2), following the manufacturer's instructions. The affinity column was then washed with successive buffers: 150 mm NaCl, 20 mm Tris-HCl; 400 mm NaCl, 20 mm Tris-HCl; 150 mm NaCl, 20 mm Tris-HCl; and 20 mm Tris-HCl (pH 8.0). Bound MHC complex subunits were eluted in 0.1 M acetic acid and subjected to desalting using prewashed SepPac-C18 cartridges (Waters, WAT054960). Peptides were finally purified from the MHC class I protein chains through elution with 30% and 40% acetonitrile in 0.1% trifluoroacetic acid and dried using vacuum centrifugation (Eppendorf).

LC-MS analysis of MHC-I peptides

LC-MS analysis of MHC-I peptides was conducted following previously described protocols[14] with the following exceptions: dispensing/aspiration time was 10 prior to sample injection, sample loading pressure was set to 700 bar, gradient flow rate was 150 nL/min for 30 min, mass range was 100–700 m/z and mobility range was 0.6–1.70 V.s/cm,^{2} and intensity threshold was 500. Advanced collision energy settings consisted of nine points of collision energy dependency on ion mobility: 0.70 V.s/cm^2 - 27.50 eV; 0.85 V.s/cm^2 - 32.00 eV; 0.90 V.s/cm^2 - 36.00 eV; 0.95 V.s/cm^2 - 38.00 eV; 1.25 V.s/cm^2 - 44.00 eV; 1.30 V.s/cm^2 - 46.00 eV; 1.35 V.s/cm^2 - 47.00 eV; 1.50 V.s/cm^2 - 47.00 eV; 1.65 V.s/cm^2 - 50.00 eV.

Proteomics database search

All MS/MS spectra were searched by PEAKS Studio 11.0 (build 20,230,414, BSI) using a Deep Novo search (database-free de novo search) followed by a Peptide Search (database search with target-decoy strategy). UniProt Human reference proteome database was used (including isoforms 103,789 entries, downloaded from uniprot.org on 26th April 2023). This reference database was concatenated either with a list of 113 celltron MHC-neoepitopes protein entries or with 40,409 protein entries from cosmic mutanome database for specific searches. A precursor mass tolerance of 20 ppm and a fragment ion mass tolerance of 0.05 Da were used. Enzyme was none, digest mode unspecific, and oxidation of methionine was used as variable modification, with max two oxidations per peptide. An FDR cutoff of 5% was employed at the peptide level. The mass spectrometry proteomics data have been deposited to the ProteomeXchange Consortium via the PRIDE partner repository with the dataset identifier PXD051880.

Peptide selection

Our internally developed and publicly available homology evaluation of xenopeptides (HEX) software[15] was further applied for identification of tumor-specific peptides. The list of identified peptides was reviewed for 1) HLA binding affinity, 2) predicted prognostic RCC markers and 3) overlap with previously detected peptides from ccRCC surgery-derived cell cultures (unpublished data). A total of 11 selected peptides were then ordered from Chempeptide (China).

Peptide list: HPQVVILSL, ILGPMFSGK, RLFESSFHY, RVYNNTARY, SPSPSGSVL, SPSSILSTL, RPIGIGVQGL, ESYSVYVYK, YFDPANGKF, RPWLEGRHTL, KKKKKKKELAGIGILTV.

ELISpot

Human IFN-γ Single-Color ELISpot (Immunospot) was performed for selected peptides with PBMCs from HLA-typed buffy coats of three healthy donors (Donor-1, Donor-2, and Donor-3). PBMC purification was performed as stated above. 2 µg of peptide was incubated together with 3×10^5 isolated PBMCs for 24 h at +37°C and 5% CO_2. Assay development was performed according to manufacturer´s protocol.

Peptide-specific T-cell generation

Microbeads for CD14 (Miltenyi Biotec, Cat#130-097-057) and CD8 (Miltenyi Biotec, Cat#130-097-052) were used to isolate monocytes and T-cells from PBMCs, respectively. Monocytes were differentiated with GM-CSF (1000 U/ml) and IL-4 (800 U/ml) for 4 days. Differentiated monocyte-derived dendritic cells were then pulsed for 2 h at 37°C with selected peptides (10 μM), then incubated 4 h with TNFa (10 ng/ml, Peprotech, Cranbury, NJ) and LPS (10 ng/ml) for DC maturation and finally co-cultured with autologous CD8+ T cells at a 1:10 ratio. Re-stimulation of the same T-cells was done after 10–12 days using freshly peptide-pulsed monocytes. Cells were fed with IL-2 (50 U/ml, STEMCELL Technologies) or IL-15 (10 ng/ml, R&D Systems) every 2–3 days.

Ethical considerations

All patient material and clinical data were obtained as part of Development of Diagnostics and Treatment of Urological Cancers (DEDUCER) under Institutional Ethical Review Board-approved protocol and in accordance with the Declaration of Helsinki. The study was conducted in accordance with patient 's consent and study-specific ethical committee approvals 15.03.2017 (154/13/03/02/2016) and 14.7.2021 (reference HUS/850/2017) and hospital research permits: HUS/71/2017 (26.04.2017) and HUS/155/2021 (26.8.2021). The principles relating to the processing of personal data (GDPR) are considered in all data annotation and handling procedures.

All animal experiments were reviewed and approved by the Experimental Animal Committee of the University of Helsinki and the Provincial Government of Southern Finland (license number ESAVI/11895/2019).

The use of biobank donor samples is in accordance with the biobank consent and meets the requirements of the Finnish Biobank Act 688/2012.

Results

CXCL9, CXCL10 and IL-15 expressing viruses retain oncolytic fitness across ccRCC cell models

We evaluated the adenovirus constructs expressing CXCL9, CXCL10, and IL-15 (Figure 1(a)) for their immunotherapeutic potential and effect on T-cell migration in different ccRCC tumor models. Initially, we assessed the expression levels of each cytokine-encoding transgene in the 786-O cell line, Pt-1, Pt-2 and Pt-3 cells and observed high levels of CXCL9, CXCL10 and IL-15 cytokines (Figure 1(b-d)). Cell viability was then evaluated in 786-O (Figure 1(e)) and three different PDC cultures after viral infection (Figure 1f-h). In all models, a consistent trend emerged, revealing nearly 100% lysis at the highest virus concentration, alongside reduced cell viability with Ad5/3-IL-15 at elevated viral particle concentrations compared to the other viruses. However, the cell viability dropped to ~50% for all patient-derived cultures at a concentration one log lower compared to the cell line. The viral replication pattern was comparable in PDCs, whereas a plateau was reached earlier in 786-O cells (Figure 1(i-l)).
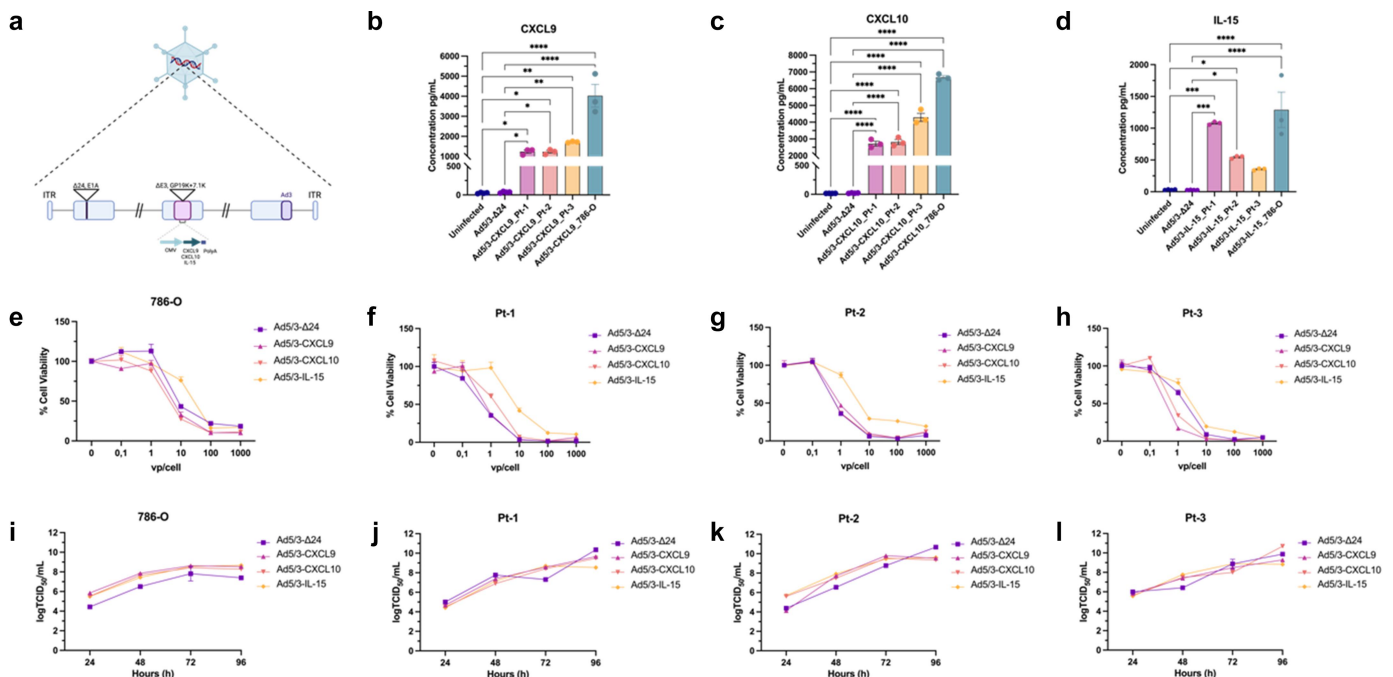

Figure 1. Characterization of oncolytic fitness in CXCL9, CXCL10 and IL-15 expressing viruses. Schematic representation of Ad5/3-Δ24 genome with transgenes encoding for CXCL9, CXCL10 or IL-15 cytokines (a). Transgene expression levels of CXCL9 (b), CXCL10 (c) and IL-15 (d) cytokines in 786-O, Pt-1, Pt-2 and Pt-3 derived cells. Cell viability was determined by MTS in 2D after 72 h in 786-O (e), Pt-1 (f), Pt-2 (g) and Pt-3 (h) derived cells. Quantification of viral infection in 786-O (i), Pt-1 (j), Pt-2 (k) and Pt-3 (l) derived cells with $TCID_{50}$ assay. Due to space constraints, only statistical significance of CXCL9, CXCL10 and IL-15 cytokines compared to MOCK and Ad5/3-Δ24 are shown (b-d). $*p < 0.05$, $**p < 0.01$, $***p < 0.001$ and $****p < 0.0001$ (two-way ANOVA).

CXCR3 receptor-ligand pair facilitates immune cell migration

High chemokine secretion prompted further investigation of gradient-dependent T-cell migration. Initially, we determined CD4+ and CD8+ T-cell proportions within CD3+ lymphocytes in healthy-donor human PBMCs (Figure 2(a)). Flow cytometry analysis (Supplementary Figure S1A) revealed CD4+ and CD8+ T-cells to constitute 55% and 45% of CD3+ cells, respectively. We observed variation in the percentage of CXCR3 receptor expression across CD3+, CD4+ and CD8+ populations. However, the mean fluorescence intensity (MFI) of CD3+_CXCR3+, CD4+_CXCR3+ and CD8+_CXCR3+ cells was consistently higher compared to the MFI of respective parental (CD3+, CD4+ and CD8+) population (Figure 2(b-d)). To assess PBMC migration in vitro, we employed a resistance-based transwell migration assay (Figure 2(e)) using filter inserts of 5 μm diameter pore size to mimic tissue resistance[16] (Supplementary Figure S5A) in 786-O and Pt3-derived cancer cells (Figure 2(f-g)) by flow cytometry (Supplementary Figure S1B-C), respectively. Immune cell migration was always greater in cells infected with cytokine-encoding viruses compared to MOCK and Ad5/3-Δ24 controls and notably higher in PDCs compared to 786-O. However, infection with virus combinations did not result in increased migration (Figure 2(f)).

Immune cell infiltration increases following treatment with cytokine-armed viruses in immunocompromised mice

To investigate cytokine-based migration in vivo, we injected 786-O cells and human PBMCs into immunodeficient mice. Established 786-O tumors were treated with Ad5/3-Δ24, Ad5/3-CXCL9, Ad5/3-CXCL10 or Ad5/3-IL-15 viruses as scheduled (Figure 3(a)). Intratumoral endpoint analysis revealed significantly higher CD3+, CD4+ and CD8+ T-cell infiltration with virus treatment compared to MOCK controls (Figure 3(b-e), Supplementary Figure S2), except for CD3+ cells in Ad5/3-Δ24 and Ad5/3-IL-15 groups (Figure 3(b)). The hypothesis of increased T-cell infiltration due to cytokine secretion in vitro was supported by observations that the Ad5/3-Δ24-treated group attracted fewer CD3+, CD4+ and CD8+ T-cells. Additionally, CXCL9 and CXCL10 outperformed IL-15 in attracting CD3+ and CD4+ T-cells (Figure 3(b-c)). mIHC staining (Figure 3(f)) and single-channel images (Supplementary Figure S3A-B) revealed high levels of immune cell infiltration in mouse tumors, particularly in Ad5/3-CXCL9, Ad5/3-CXCL10 and Ad5/3-IL-15 treated groups. The Ad5/3-Δ24-treated sample also showed infiltration of CD4+ helper T-cells (blue), as expected due to the immunogenic nature of the adenovirus.[10,17] The second round of mIHC staining (2) showed CD45+ cells in the core of tissues treated with Ad5/3-CXCL9, Ad5/3-CXCL10 and Ad5/3-IL-15, while Ad5/3-Δ24-treatment resulted in CD45+ cells mostly gathering at the tissue border.
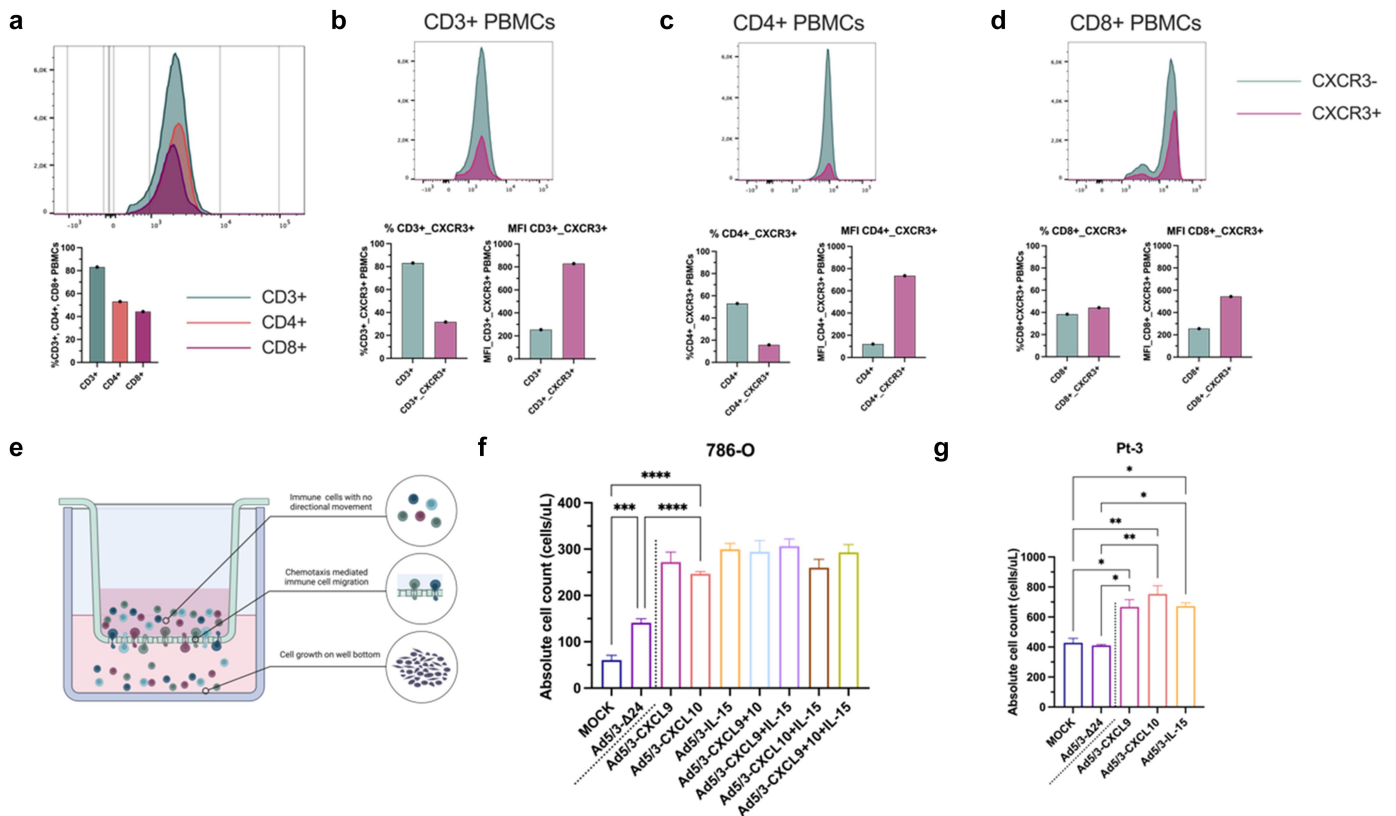
Figure 2. CXCR3 receptor expression on human PBMCs and PBMC migration in transwell system. Proportion of human CD3+, CD4+ and CD8+ cell populations in healthy-donor PBMCs (a). Further analysis from (a) reveals CXCR3 receptor expression in percentages and MFI on PBMCs (b), CD4+ (c) and CD8+ (d) cells, respectively. Schematic representation of the transwell experiment set-up (e). Migration of PBMCs in response to 786-O cells (f) and Pt-3 derived cells (g) infected with single, and/or combinations of Ad5/3-Δ24, Ad5/3-CXCL9, Ad5/3-CXCL10 and Ad5/3-IL-15 expressing viruses in the transwell system after 72 h. Due to limited space, we only show significance levels of Ad5/3-CXCL10 condition compared to MOCK and Ad5/3-Δ24 as reference (f). Significance between MOCK or Ad5/3-Δ24 with any other treatment group was ***$p < 0.001$ or ****$p < 0.0001$ (f) and *$p < 0.05$ or **$p < 0.01$ (g) (two-way ANOVA).
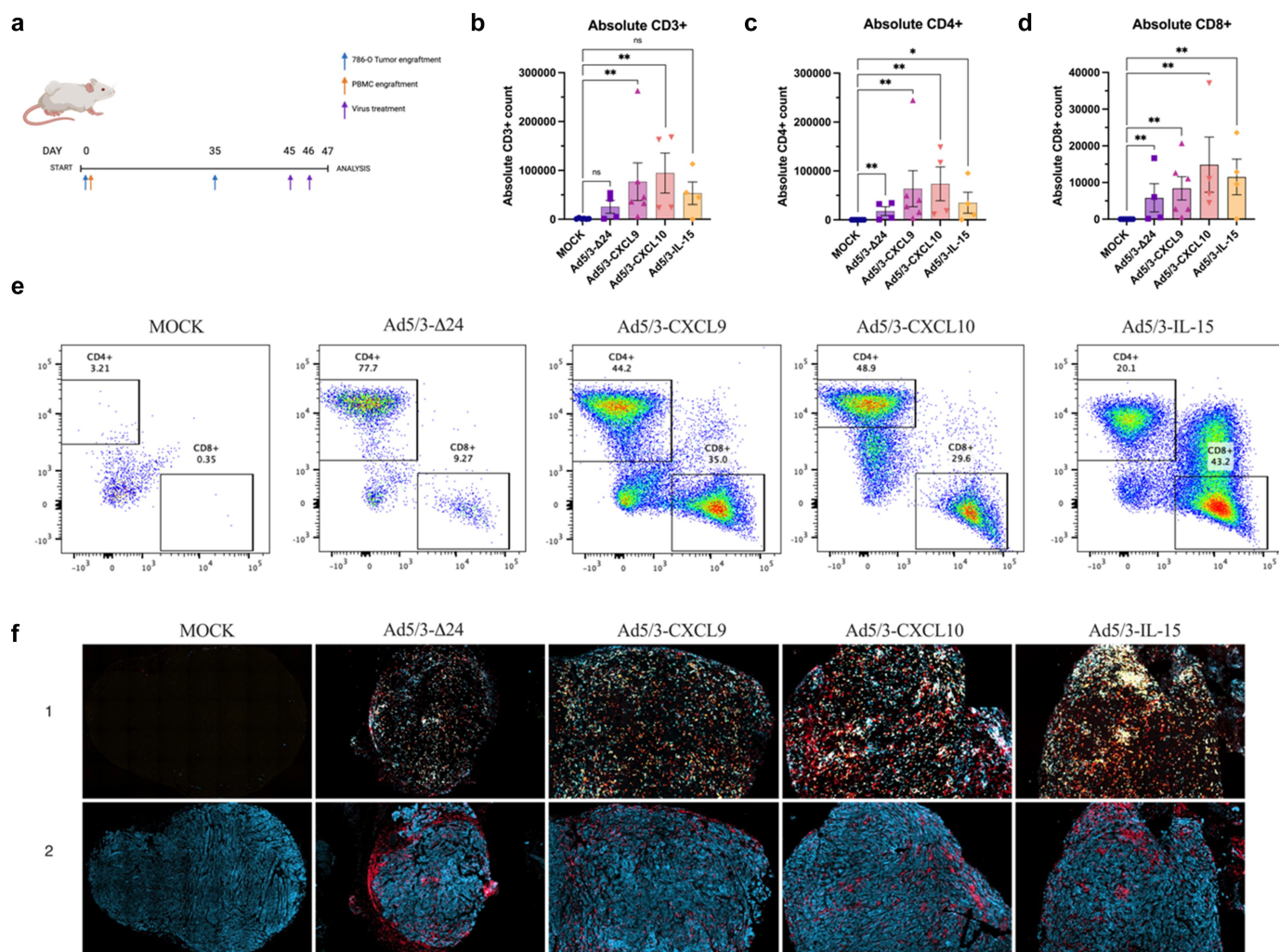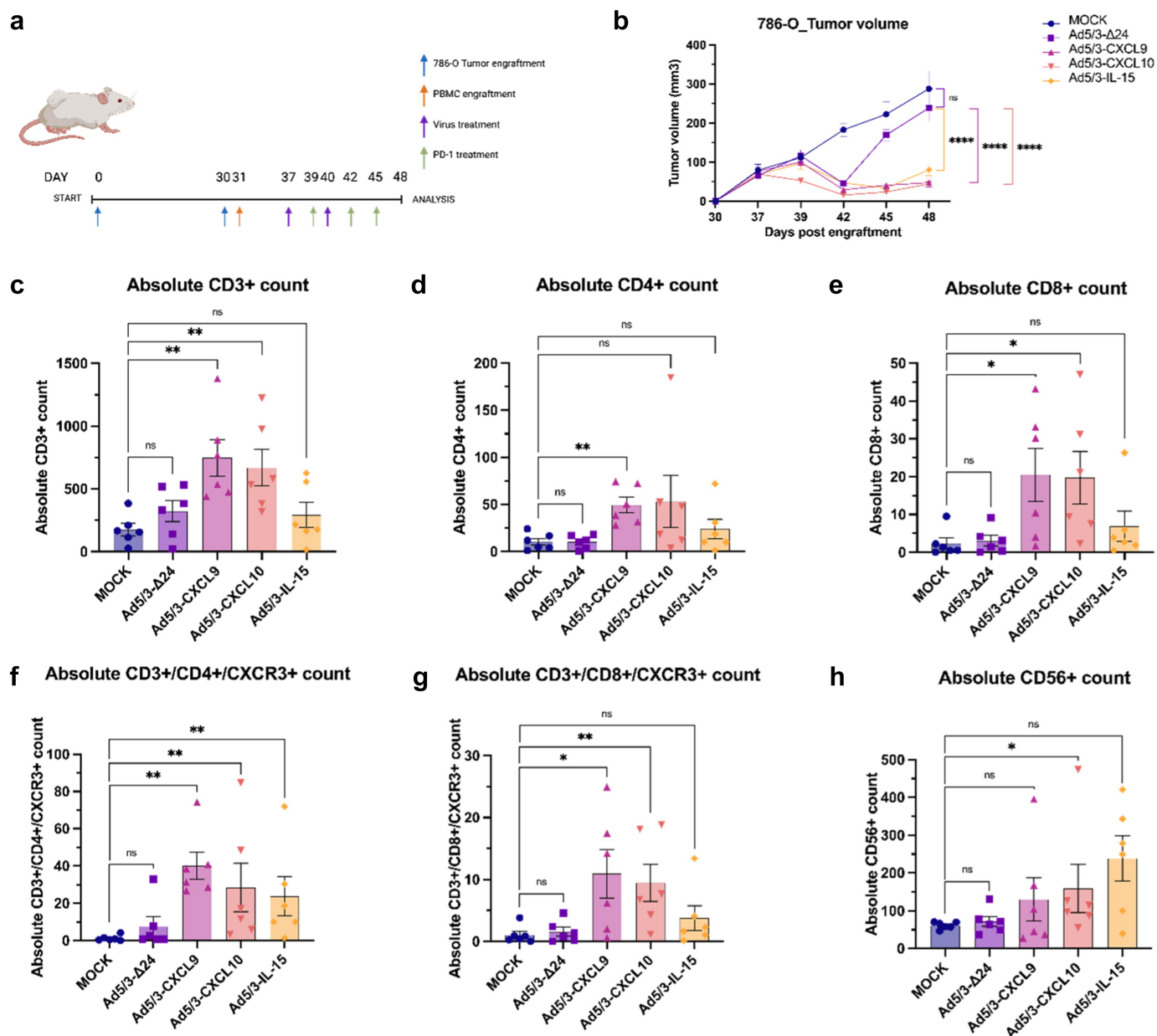
Figure 3. Migration of PBMCs in in vivo mouse models treated with oncolytic adenovirus. Schematic representation of the treatment schedule (a) in immunocompromised mice. Tumors were collected at the experimental endpoint and absolute CD3+ (b), CD4+ (c) and CD8+ (d) cell counts in the TME of mouse tumor samples were analyzed by flow cytometry. Representative CD4+ and CD8+ T-cell populations (e) and mIHC images (f) of each treatment group are shown for the first (1) and second (2) round of staining. Markers for DAPI (white), FOXP3 (green), CD3 (orange), CD4 (blue) and CD8 (red) were stained in the first round followed by CD45 (red), CAIX + E cadherin + pan Cytokeratin (blue) staining in the second round. ns $p > 0,05$, *$p < 0.05$ and **$p < 0.01$ (Mann–Whitney test with SEM).

Treatment with cytokine-armed viruses and anti-PD-1 enhances the migration of T-cells and nk-cells in immunocompromised mice

After observing increased immune cell infiltration in immunocompromised 786-O tumor bearing mice, we further investigated the efficacy of our cytokine-armed viruses in combination with anti-PD-1 treatment. Based on earlier findings (Figure 3, Supplementary Figure S3), we hypothesized that viral treatment might recruit additional immune cell populations beyond T-cells to the TME, and that anti-PD-1 could effectively control tumor growth. We focused on exploring NK-cell infiltration, given that the CXCR3 chemokine receptor is typically expressed on NK-cells. As before, 786-O cells were injected to establish subcutaneous tumors, and human PBMCs were used to create circulating immune cells of human origin in the immunocompromised mouse model. Mice received group-specific treatment with Ad5/3-Δ24, Ad5/3-CXCL9, Ad5/3-CXCL10, or Ad5/3-IL-15 viruses, along with scheduled

anti-PD-1 treatment (Figure 4(a)). The combination of Ad5/3-CXCL9, Ad5/3-CXCL10, and Ad5/3-IL-15 with anti-PD-1 effectively controlled tumor growth compared to Ad5/3-Δ24 or MOCK-treated mice (Figure 4(b)). Flow cytometry analysis at the study endpoint revealed greater infiltration of CD3+, CD4+, and CD8+ T-cells in tumors treated with Ad5/3-CXCL9, Ad5/3-CXCL10 and Ad5/3-IL-15 compared to MOCK controls (Figure 4(c-e)), consistent with previous observations. Notably, T-cell migration was highest in Ad5/3-CXCL9 and Ad5/3-CXCL10 treated tumors, prompting further investigation into CXCR3+ T-cell subsets in the TME. Indeed, CXCR3+ CD4+ and CXCR3+ CD8+ T-cells were significantly more abundant in virus-treated tumors, particularly in those treated with Ad5/3-CXCL9 and Ad5/3-CXCL10 (Figure 4(f-g)). CD56+ NK-cells also increased across all groups treated with cytokine-armed virus, but unlike T-cells, the highest number of intratumoral NK-cells was observed in Ad5/3-IL-15 treated tumors (Figure 4h).

Figure 4. Migration of PBMCs in in vivo mouse models treated with oncolytic adenovirus and anti-PD-1. Schematic representation of the treatment schedule (a) in immunocompromised mice treated intratumorally with either Ad5/3-Δ24, Ad5/3-CXCL9, Ad5/3-CXCL10, Ad5/3-IL-15 expressing viruses, or no viral treatment (MOCK). All mice received anti-PD-1 intraperitoneally on the specified treatment days as indicated. Tumor volume was recorded every 2–3 days, starting from day 30 (b), and continued until the study endpoint when tumors were collected and analyzed by flow cytometry. The absolute cell counts of migrated CD3+ (c), CD4+ (d), and CD8+ (e) T-cells in the TME of mouse tumor samples are shown. CXCR3 receptor expression was further assessed on both CD4+ (f) and CD8+ (g) T-cell subsets. Additionally, absolute numbers of CD56+ NK-cells (h) were measured in the TME across all treatment groups. Statistical significance of Ad5/3-CXCL9, Ad5/3-CXCL10 and Ad5/3-IL-15 groups compared to Ad5/3-Δ24 and MOCK was the same, and therefore only shown for Ad5/3-Δ24 treated mice (B) with significance levels set at *p <0.05, **p <0.01, ***p <0.001 and ****p <0.0001 (two-way ANOVA). Significance for all flow cytometry analysis (C-H) was ns p>0.05, *p <0.05 and **p <0.01 (Mann–Whitney test with SEM).

Adenoviral infection enhances immune cell migration in tumor organoids

Characterization of malignant kidney-derived cells was demonstrated through immunofluorescence staining of 2D PDCs (Figure 5(a-c)) and 3D PDOs (Figure 5(d-f)) for Pt-1, Pt-2 and Pt3. 2D cultures stained for CAIX, Vimentin, Cytokeratin, E-Cadherin, Phalloidin and DAPI show weak E-Cadherin signal, often observed in ccRCC. Phalloidin, CAIX, vimentin, and pan-cytokeratin showed consistent epithelial marker expression across all cell models, indicating intact cellular structure.

Following the ability of oncolytic adenoviruses to infect PDCs in 2D (Figure 1(f-h)), we sought to explore infectivity in 3D PDOs over time, utilizing an RFP expressing virus for visualization (Figure 5(g)). For improved clinical relevance of cytokine expressing viruses, we assessed chemoattraction-based PBMC migration using a microfluidic chip system (Figure 5(h-i), Supplementary Figure S5B). Visual presentation of sample chambers at 0–48 h showed PBMC migration (green) over time (Figure 5(h-i)). Following the release of CXCL9 and CXCL10, immune cell migration significantly increased in Ad5/3-CXCL9 conditions compared to Ad5/
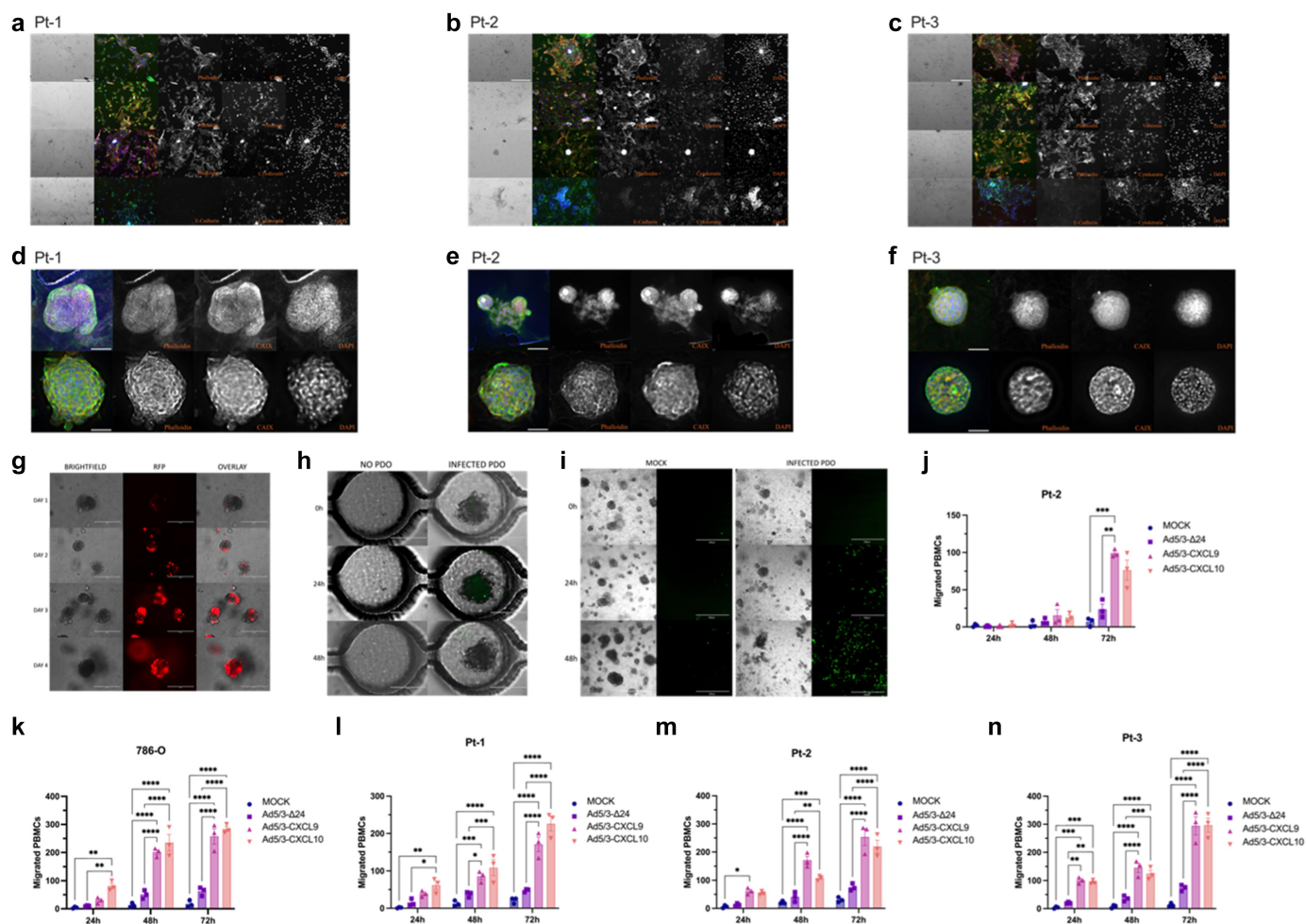
Figure 5. Immunofluorescence staining, Ad5-Δ24-RFP infection and PBMC migration in PDOs. PDCs were immunostained in 2D (a-c) and 3D (d-f) for characterization of CAIX, Vimentin, pan Cytokeratin, E-Cadherin and Phalloidin expression in Pt-1 (a, d), Pt-2 (b, e) and Pt-3 (c, f) cells. Replicate conditions are shown row-wise for each patient. PDOs infected with Ad5-Δ24-RFP at MOI 100 show the capability and gradual progression of infection over time (g). Fluorescently labeled PBMCs that migrated in PDO sample chambers were visualized on a microfluidic glass slide chip (h) and Plate 96-Single chip (i) at 0 h, 24 h, and 48 h after infection. The number of migrated cells in response to infection-induced cytokine release is shown for Pt-2 PDOs on the microfluidic glass slide chip (j) and for 786-O organoids and Pt 1–3 PDOs on the Plate 96-Single chip (k-n). Statistical significance of Ad5/3-CXCL9 and Ad5/3-CXCL10 compared to MOCK and Ad5/3-Δ24 is shown for all time points (j-n). *p <0.05, **p <0.01, ***p <0.001 and ****p <0.0001 (two-way ANOVA with SEM). Scale bars represent 300 μm (a-c), 150 μm upper row and 50 μm bottom row (d-f), 400 μm (g-h) and 500 μm (l).

3-Δ24 and MOCK controls after 72 h in Pt-2 PDOs on the glass slide chip (Figure 5(j)). On the Plate 96-Single chip, a significant increase in migrated PBMCs in one or both Ad5/3-CXCL9 and Ad5/3-CXCL10 conditions was observed as early as 24 h after infection, with further increases up to 72 h, depending on whether 786-O organoids or Pt 1–3 PDOs were used (Figure 5(k-n)).

Renal cancer peptides trigger immune reactivity in HLA-typed PBMCs

After verifying the suitability of oncolytic adenoviruses for PDC therapy, we sought to enhance therapy with tumor-associated antigens (TAAs). 786-O cells underwent immuno-peptidomics analysis to evaluate the therapeutic potential as cancer vaccine targets (Supplementary Figure S6). We first assessed HLA-A,B,C+ and PD-L1 expression levels (Figure 6 (a-b)) observing high expression of each marker. MS-based peptide identification revealed peptide distribution where 9–10-mers accounted for ~53%, with 9-mers comprising

~35% and 10-mers ~18% (Figure 6(C)). Evaluation of peptide binding to HLA haplotypes (HLA-A03:01, HLA-B07:02, HLA-B44:02, HLA-C05:01, HLA-C07:02) further indicated that 9- and 10-mers bind approximately 90% and 80% of the total peptide count (Figure 6(d)). HLA-binding peptides were classified as strong, weak, or non-binders and deconvoluted for each HLA haplotype (Figure 6(e)). Ten peptides selected as previously mentioned were then assessed for their potential to induce immune reactivity in HLA-typed PBMCs of three healthy-donor subjects (Figure 6(f-h)). Donor-1 (Figure 6(f)) showed similar traits to Donor-3 (Figure 6(h)), where peptides 1 and 7 outperformed all other peptides, including our positive poly-K MART-1, and negative PBMC control. Peptide-specific responses in PBMCs from Donor-2 (Figure 6(g)) did not reach significance. Consequently, we chose to proceed with peptide pulsing of CD8+ T-cells using peptides 1 and 7. Finally, when determining cell viability of infected target cells without peptide-pulsed CD8+ effector cells, significant differences were only observed following adenoviral infection with Ad5/3-CXCL9 (Figure 6i). However, peptide-pulsed CD8+ T-cells
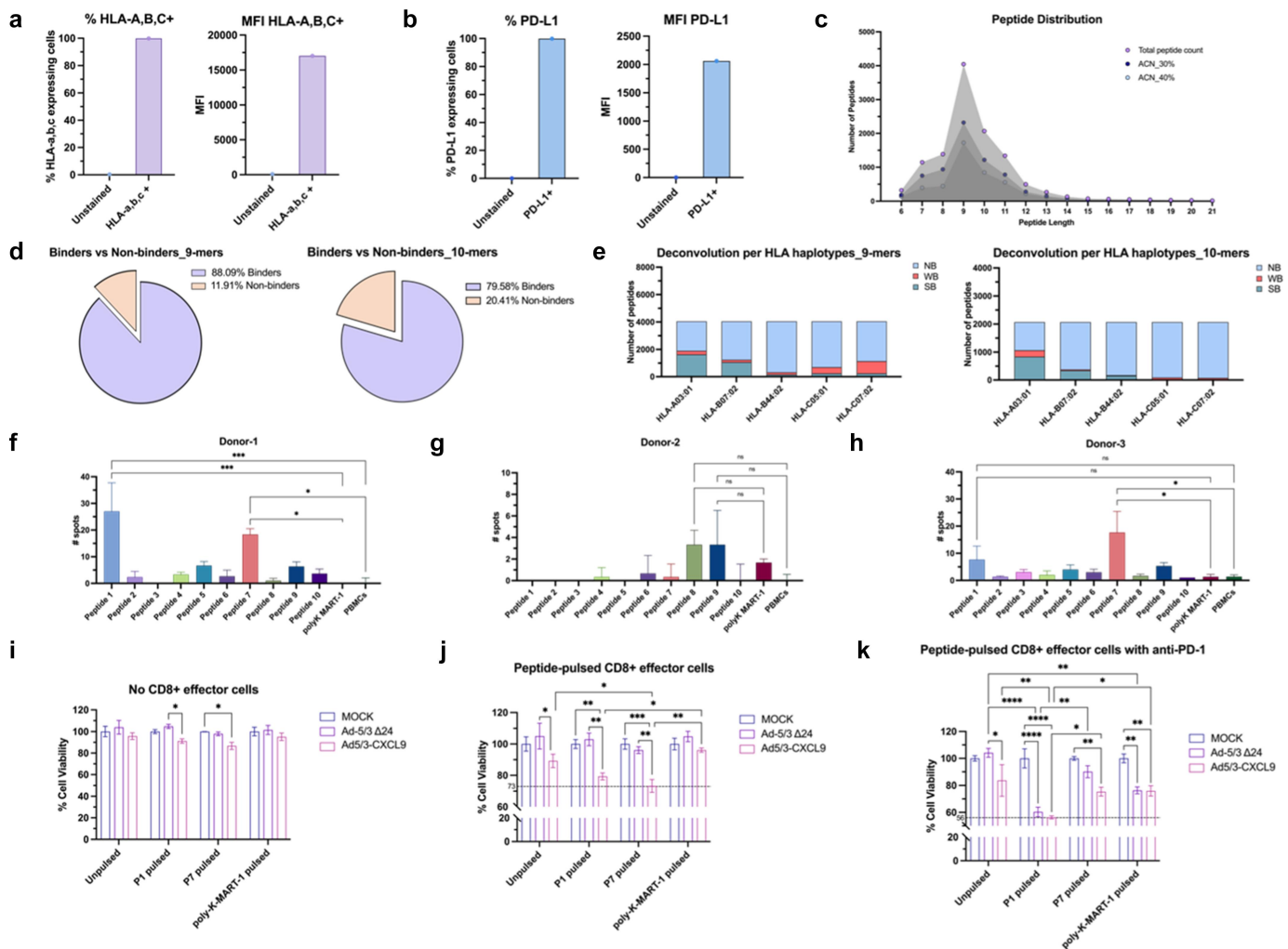
Figure 6. Peptide distribution, response and killing of ccRCC cells. Number and respective MFI of HLA-A,B,C (a) and PD-L1 (b) expressing 786-O cells. Peptide distribution based on length and quantity (c) of binders vs non-binders to the relevant HLAs of identified peptides (d) were deconvoluted into strong binders (SB), weak binders (WB) and non-binders (NB) based on 786-O cell line HLA haplotypes (e). Peptide immunogenicity revealed by human IFNγ ELISpot for selected peptides in three different HLA-typed healthy-donor buffy coats (f, g, h), respectively. Killing ability of pulsed CD8+ T-cells was determined by cell viability in response to viral infection and presence of no CD8+ effector cells (i), peptide-pulsed CD8+ effector cells (j) and peptide-pulsed CD8+ effector cells in combination with anti-PD-1 (k). ns $p > 0,05$, *$p < 0.05$, **$p < 0.01$, ***$p < 0.001$ and ****$p < 0.0001$ (one-way or two-way ANOVA).

significantly enhanced target cell killing when combined with viral infection alone (Figure 6(j)) and even more so when combined with anti-PD-1 treatment (Figure 6(k)). Notably, Ad5/3-CXCL9 was more potent in eliciting tumor cell killing across most experimental conditions (Figure 6(i-k)).

Discussion

In our current study, we observed increased immune cell infiltration in ccRCC models, of both 2D and 3D *in vitro* cultures, as well as *in vivo* mice, due to oncolytic adenovirus infection and cytokine secretion within the TME. Coinciding with previous studies,[12,18–21] we showed that cytokines of C-X-C Motif Chemokine Ligands subjectively contribute to the attraction and movement of human immune cells toward malignant cells when exposed to oncolytic adenoviruses. Building on this understanding, the combination of CXCR3 receptor-ligand signaling with ICIT has been proposed to enhance the efficacy of PD-1 therapy.[19,22–24] In this context, we observed increased immune cell infiltration in vivo

following treatment with adenovirus in combination with anti-PD-1. Additionally, there was enhanced target cell killing by ccRCC TAA-peptide-pulsed CD8+ T-cells in the presence of anti-PD-1 and Ad5/3-CXCL9 virus, compared to cultures without PD-1.

Our data demonstrate that the CXCL9/CXCL10/CXCR3 axis plays a crucial role in immune cell migration in both in vitro and in vivo human ccRCC tumor models. The release of these cytokines following viral infection with Ad5/3-CXCL9 and Ad5/3-CXCL10 triggers strong antitumor immune responses and enhances therapeutic efficacy by promoting immune cell migration to the tumor. Consistent with this, we observed increased T-cell migration toward Ad5/3-CXCL9 and Ad5/3-CXCL10 treated tumors in vivo, while NK-cell migration was more prominent in tumors treated with Ad5/3-IL-15. These observations align with previously reported effects of these cytokines, where CXCL9 and CXCL10 effectively attract T-cells, while IL-15 is essential for NK-cell survival, activation, and chemotaxis.[25–27] Additionally, the reduced tumor growth observed in mice treated with Ad5/3-CXCL9, Ad5/3-CXCL10,

and Ad5/3-IL-15 supports the notion that presence of immune cells in the TME is crucial for improving treatment outcomes. In this study, we focused specifically on T-cells and NK-cells. However, future research should explore a broader range of immune cell populations in the TME after treatment with cytokine-armed viruses in immunocompromised mice, to gain a detailed understanding of which immune cells are present in the tumor, their activation status, and how these factors influence antitumor activity.

Combination therapies utilizing cytokine-armed oncolytic viruses to augment antitumor responses in solid tumors[28] have, alongside peptide vaccination based on HLA class I and II ligands in ccRCC,[29] gained attention over the years. Yet, the potential synergy between vaccination approaches involving oncolytic adenoviruses encoding for CXCR3 ligands and ccRCC tumor peptides remains unexplored. Our study addresses this gap by demonstrating that adenoviral infection induces cytokine secretion and T-cell trafficking and that they, together with immunogenic tumor peptides, could provide a potential vaccination approach for ccRCC. Furthermore, *in vitro* peptide-based T-cell priming significantly increased the killing of ccRCC target cells.

By integrating cytokine secretion-mediated T-cell trafficking with the PeptiCRAd vaccination strategy, which uses tumor peptide-coated viruses, our findings suggest a novel approach for generating tumor antigen-specific immune responses in virus-infected ccRCC tumors *in vivo*. This approach, which is set for further validation, could potentially enhance the therapeutic potential of the PeptiCRAd technology by incorporating our cytokine-encoding adenoviruses. However, while numerous studies have explored clinically applicable combination strategies for the treatment of cancer, no single therapeutic approach has consistently demonstrated superiority over others, emphasizing an ongoing search for broader cancer strategies.

Here, our peptide discovery focused on the 786-O ccRCC cell line as a model, paving the way for future ligandome analysis on surgically removed fresh ccRCC tissue to improve representativeness of the patient-specific peptide repertoire. This approach would involve analyzing HLA-presented peptides from nonmalignant tissue and PBMCs as controls to ensure that identified peptides are specific to the tumor tissue.

Notably, Klatt et al. performed exclusion of overlapping peptides in ccRCC tumors and PBMCs due to the likelihood of tumor lymphocyte infiltration, thereby improving the comparative analysis of malignant vs nonmalignant antigen expression repertoire.[29] Although conducting a comparative peptide analysis of our identified peptides and PBMCs from responding HLA-matched subjects would be intriguing, we successfully demonstrated the immunogenicity and cytotoxic potential of the top-performing peptides (peptide 1 and peptide 7) through *in vitro* assays in 786-O cells. Overall, our ligandome analysis pipeline identified potential therapeutic peptide targets for ccRCC and experimentally validated their immunogenic potential. However, careful validation is necessary to assess the clinical applicability of identified peptides in PDCs, whether used alone or in combination with therapies such as adenoviruses or ICIs, before implementing HLA-binding peptide therapies in patients.

ORCID

Vincenzo Cerullo (iD) http://orcid.org/0000-0003-4901-3796

Data availability statement

The authors confirm that all manuscript data are available in the main text and supplementary material. Raw data of this study are available upon reasonable request from the corresponding author. The mass spectrometry proteomics data have been deposited to the ProteomeXchange Consortium via the PRIDE partner repository with the dataset identifier PXD051880.

References

1. Mahoney KM, Rennert PD, Freeman GJ. Combination cancer immunotherapy and new immunomodulatory targets. Nat Rev Drug Discov. 2015;14(8):561–584. doi:10.1038/nrd4591.
2. Fridman WH, Pagès F, Sautès-Fridman C, Galon J. The immune contexture in human tumours: impact on clinical outcome. Nat Rev Cancer. 2012;12(4):298–306. doi:10.1038/nrc3245.
3. Galon J, Costes A, Sanchez-Cabo F, Kirilovsky A, Mlecnik B, Lagorce-Pagès C, Tosolini M, Camus M, Berger A, Wind P. et al. Type, density, and location of immune cells within human colorectal tumors predict clinical outcome. Sci (1979). 2006;313 (5795):1960–1964. doi:10.1126/SCIENCE.1129139/SUPPL_FILE/GALON.SOM.PDF.
4. Kohli K, Pillarisetty VG, Kim TS. Key chemokines direct migration of immune cells in solid tumors. Cancer Gene Ther. 2022;29 (1):10–21. doi:10.1038/s41417-021-00303-x.
5. Chheda ZS, Sharma RK, Jala VR, Luster AD, Haribabu B. Chemoattractant receptors BLT1 and CXCR3 regulate antitumor immunity by facilitating CD8 + T cell migration into tumors. The

J Immunol. 2016;197(5):2016–2026. doi:10.4049/jimmunol.1502376.

6. Groom JR, Luster AD. CXCR3 in T cell function. Exp Cell Res. 2011;317(5):620–631. doi:10.1016/J.YEXCR.2010.12.017.

7. Waldmann TA. The biology of interleukin-2 and interleukin-15: implications for cancer therapy and vaccine design. Nat Rev Immunol. 2006;6(8):595–601. doi:10.1038/nri1901.

8. Kovanen PE, Leonard WJ. Cytokines and immunodeficiency diseases: critical roles of the γc-dependent cytokines interleukins 2, 4, 7, 9, 15, and 21, and their signaling pathways. Immunol Rev. 2004;202(1):67–83. doi:10.1111/J.0105-2896.2004.00203.X.

9. Ylösmäki E, Cerullo V. Design and application of oncolytic viruses for cancer immunotherapy. Curr Opin Biotechnol. 2020;65:25–36. doi:10.1016/j.copbio.2019.11.016.

10. Feola S, Russo S, Ylösmäki E, Cerullo V. Oncolytic ImmunoViroTherapy: a long history of crosstalk between viruses and immune system for cancer treatment. Pharmacol Ther. 2022;236:108103. doi:10.1016/J.PHARMTHERA.2021.108103.

11. Capasso C, Hirvinen M, Garofalo M, Romaniuk D, Kuryk L, Sarvela T, Vitale A, Antopolsky M, Magarkar A, Viitala T. et al. Oncolytic adenoviruses coated with MHC-I tumor epitopes increase the antitumor immunity and efficacy against melanoma. Oncoimmunology. 2016;5(4):e1105429. doi:10.1080/2162402X.2015.1105429.

12. Hamdan F, Martins B, Feodoroff M, Giannoula Y, Feola S, Fusciello M, Chiaro J, Antignani G, Grönholm M, Ylösmäki E. et al. GAMER-Ad: a novel and rapid method for generating recombinant adenoviruses. Mol Ther Methods Clin Dev. 2021;20:625–634. doi:10.1016/J.OMTM.2021.01.014.

13. Scholtalbers J, Boegel S, Bukur T, Byl M, Goerges S, Sorn P, Loewer M, Sahin U, Castle JC. TCLP: an online cancer cell line catalogue integrating HLA type, predicted neo-epitopes, virus and gene expression. Genome Med. 2015;7(1):118. doi:10.1186/S13073-015-0240-5.

14. Chiaro J, Antignani G, Feola S, Feodoroff M, Martins B, Cojoc H, Russo S, Fusciello M, Hamdan F, Ferrari V. et al. Development of mesothelioma-specific oncolytic immunotherapy enabled by immunopeptidomics of murine and human mesothelioma tumors. Nat Commun. 2023;14(1):7056. doi:10.1038/s41467-023-42668-7.

15. Chiaro J, Kasanen HHE, Whalley T, Capasso C, Grönholm M, Feola S, Peltonen K, Hamdan F, Hernberg M, Mäkelä S. et al. Viral molecular mimicry influences the antitumor immune response in murine and human melanoma. Cancer Immunol Res. 2021;9(8):891–993. doi:10.1158/2326-6066.CIR-20-0814/665764/AM/VIRAL-MOLECULAR-MIMICRY-INFLUENCES-THE-ANTITUMOR.

16. Chiu PL, Chang CH, Lin YL, Tsou PH, Li BR. Rapid and safe isolation of human peripheral blood B and T lymphocytes through spiral microfluidic channels. Sci Rep. 2019; 8145. doi:10.1038/s41598-019-44677-3.

17. Farrera-Sal M, Moya-Borrego L, Bazan-Peregrino M, Alemany R. Evolving status of clinical immunotherapy with oncolytic adenovirus. Clin Cancer Res. 2021;27(11):2979–2988. doi:10.1158/1078-0432.CCR-20-1565.

18. Wang G, Zhang Z, Zhong K, Wang Z, Yang N, Tang X, Li H, Lu Q, Wu Z, Yuan B. et al. CXCL11-armed oncolytic adenoviruses enhance CAR-T cell therapeutic efficacy and reprogram tumor microenvironment in glioblastoma. Mol Ther. 2023;31(1):134–153. doi:10.1016/j.ymthe.2022.08.021.

19. Li X, Lu M, Yuan M, Ye J, Zhang W, Xu L, Wu X, Hui B, Yang Y, Wei B. et al. CXCL10-armed oncolytic adenovirus promotes tumor-infiltrating T-cell chemotaxis to enhance anti-PD-1 therapy. Oncoimmunology. 2022;11(1):2118210. doi:10.1080/2162402X.2022.2118210.

20. Harlin H, Meng Y, Peterson AC, Zha Y, Tretiakova M, Slingluff C, McKee M, Gajewski TF. Chemokine expression in melanoma metastases associated with CD8 + T-CeII recruitment. Cancer Res. 2009;69(7):3077–3085. doi:10.1158/0008-5472.CAN-08-2281/654525/P/CHEMOKINE-EXPRESSION-IN-MELANOMA-METASTASES.

21. Dangaj D, Bruand M, Grimm AJ, Ronet C, Barras D, Duttagupta PA, Lanitis E, Duraiswamy J, Tanyi JL, Benencia F. et al. Cooperation between constitutive and inducible chemokines enables T cell engraftment and immune attack in solid tumors. Cancer Cell. 2019;35(6):885–900.e10. doi:10.1016/J.CCELL.2019.05.004.

22. Luo R, Firat E, Gaedicke S, Guffart E, Watanabe T, Niedermann G. Cisplatin facilitates radiation-induced abscopal effects in conjunction with PD-1 checkpoint blockade through CXCR3/CXCL10-mediated T-cell recruitment. Clin Cancer Res. 2019;25(23):7243–7255. doi:10.1158/1078-0432.CCR-19-1344.

23. Han X, Wang Y, Sun J, Tan T, Cai X, Lin P, Tan Y, Zheng B, Wang B, Wang J. et al. Role of CXCR3 signaling in response to anti-PD-1 therapy. EBioMedicine. 2019;48:169–177. doi:10.1016/j.ebiom.2019.08.067.

24. Chow MT, Ozga AJ, Servis RL, Frederick DT, Lo JA, Fisher DE, Freeman GJ, Boland GM, Luster AD. Intratumoral activity of the CXCR3 Chemokine system is required for the efficacy of anti-PD-1 therapy. Immunity. 2019;50(6):1498–1512.e5. doi:10.1016/j.immuni.2019.04.010.

25. Dubois S, Conlon KC, Müller JR, Hsu-Albert J, Beltran N, Bryant BR, Waldmann TA. IL15 infusion of cancer patients expands the subpopulation of cytotoxic CD56bright NK cells and increases NK-Cell cytokine release capabilities. Cancer Immunol Res. 2017;5(10):929–938. doi:10.1158/2326-6066.CIR-17-0279.

26. Allavena P, Giardina G, Bianchi G, Mantovani A. IL-15 is chemotactic for natural killer cells and stimulates their adhesion to vascular endothelium. J Leukoc Biol. 1997;61(6):729–735. doi:10.1002/JLB.61.6.729.

27. Tokunaga R, Zhang W, Naseem M, Puccini A, Berger MD, Soni S, McSkane M, Baba H, Lenz HJ. CXCL9, CXCL10, CXCL11/CXCR3 axis for immune activation - a target for novel cancer therapy. Cancer Treat Rev. 2018;63:40. doi:10.1016/J.CTRV.2017.11.007.

28. Tanoue K, Shaw AR, Watanabe N, Porter C, Rana B, Gottschalk S, Brenner M, Suzuki M. Armed oncolytic adenovirus-expressing PD-L1 mini-body enhances antitumor effects of chimeric antigen receptor t cells in solid tumors. Cancer Res. 2017;77(8):2040–2051. doi:10.1158/0008-5472.CAN-16-1577/652542/AM/ARMED-ONCOLYTIC-ADENOVIRUS-EXPRESSING-PD-L1-MINI.

29. Klatt MG, Kowalewski DJ, Schuster H, Di Marco M, Hennenlotter J, Stenzl A, Rammensee HG, Stevanović S. Carcinogenesis of renal cell carcinoma reflected in HLA ligands: a novel approach for synergistic peptide vaccination design. Oncoimmunology. 2016;5(8):e1204504. doi:10.1080/2162402X.2016.1204504.